fibers

MDPI

Article

Strengthening Fire-Damaged Lightweight Concrete T-Beams Using Engineered Cementitious Composite with Basalt Fiber-Reinforced Polymer Grid

Haider M. Al-Baghdadi * and Mohammed M. Kadhum

Department of Civil Engineering, College of Engineering, University of Babylon, Babylon 51002, Iraq; eng.mohammed.mansour@uobabylon.edu.iq
* Correspondence: eng.haider.m@uobabylon.edu.iq

Abstract: Lightweight concrete (LWC) is a long-standing development in the area of construction materials. LWC has become increasingly important for sustainable construction due to its reduced susceptibility to cracking. However, when exposed to extreme temperatures during fires, LWC can lose its compressive strength and ductility. This study investigates the performance of lightweight expanded clay aggregate (LECA) concrete T-beams exposed to elevated temperatures. The research also focuses on the use of an engineered cementitious composite with a basalt fiber-reinforced polymer grid (ECCBFG) as a rehabilitation method for fire-damaged T-beams. Key variables considered include the concrete cover thickness (20 and 30 mm), fire exposure duration (30 and 60 min), and thickness of the ECCBFG layer. Thermocouples were installed at various points within the beams to monitor the heat gradient across the cross-section. Fourteen concrete beam specimens were tested, including control beams, fire-damaged beams, and beams strengthened with the ECCBFG layer. Key performance parameters, such as the energy absorption, cracking load, ductility index, maximum load capacity, and corresponding displacement, were analyzed. The experimental results showed that the strengthened beams outperformed the fire-damaged beams, closely matching the performance of undamaged reference beams in most aspects, except energy absorption. The findings suggest that further research is needed to optimize certain performance indicators and address challenges in strengthening fire-damaged beams.

Keywords: lightweight concrete; lightweight expanded clay aggregate; engineered cementitious composite; basalt fiber-reinforced polymer grid; fire damage

check for updates

Academic Editors: Maria C. Naoum, Nikos Papadopoulos and George Sapidis

Received: 6 November 2024
Revised: 5 December 2024
Accepted: 24 December 2024
Published: 13 January 2025

Citation: Al-Baghdadi, H.M.; Kadhum, M.M. Strengthening Fire-Damaged Lightweight Concrete T-Beams Using Engineered Cementitious Composite with Basalt Fiber-Reinforced Polymer Grid. *Fibers* **2025**, *13*, 7. https://doi.org/10.3390/fib13010007

Copyright: © 2025 by the authors. Licensee MDPI, Basel, Switzerland. This article is an open access article distributed under the terms and conditions of the Creative Commons Attribution (CC BY) license (https://creativecommons.org/licenses/by/4.0/).

1. Introduction

Lightweight concrete (LWC) has been a significant advancement in construction materials, with its origins dating back over 2000 years to ancient times, notably in Roman architecture. The development of artificial lightweight aggregates in the 19th and 20th centuries marked a breakthrough in material engineering [1]. LWC has become increasingly important for sustainable construction due to its reduced susceptibility to cracking. The elasticity in both the aggregate and the matrix enhances the bond between the two, reducing internal stresses. This results in concrete products up to 40% lighter than traditional concrete yet maintaining comparable strength [2].

The high air void content in LWC offers several advantages, such as lower thermal expansion, improved tensile capacity, and a superior strength-to-weight ratio. Recent advancements in production technology have enabled the manufacture of LWC with varying

densities and compressive strengths, ranging from low-density blocks with a maximum of 1200 kg/m^3 to high-density concrete reaching compressive strengths of up to 100 MPa [3]. However, when exposed to extreme temperatures during fires, LWC can lose its compressive strength and ductility. Temperatures above 550 °C increase internal stress due to vapor pressure in the concrete's pores, resulting in cracks of various sizes. Calcium hydroxide dehydrates, and the aggregates weaken at these elevated temperatures. Reinforced concrete loses significant mechanical properties, including stiffness and compressive strength, when heated above 700 °C, as binding elements like hydrated cement (C-S-H) begin to break down. Cracks propagate, and the bonds between the aggregates and cement paste deteriorate, leaving the structure vulnerable to both live and dead loads. These findings are consistent with the work of several researchers [4–8].

A time-temperature curve is the most basic method used to express fire exposure. Standards such as ISO 834 [9] are commonly applied to represent fire curves, and fire tests are conducted to assess the performance of structural elements under fire conditions. Furnace tests are typically used, with the temperature inside the furnace controlled according to the specified fire curve, whether a standard or a natural fire curve. Furnaces are generally equipped with instruments to detect temperature, and deformations, and perform load tests on the specimens [10]. While standard fire tests are valuable for evaluating fire resistance, real fire scenarios are influenced by factors such as ventilation, ambient conditions, material composition, boundary conditions, and the availability of fuel, which can significantly impact the fire's severity. The fire performance of concrete depends heavily on its mechanical properties, including the compressive and tensile strength, modulus of elasticity, and stress–strain response at high temperatures [11].

Structural LWC offers superior fire resistance compared to normal-weight concrete due to several inherent advantages. Firstly, it experiences a smaller reduction in strength at elevated temperatures, largely due to the thermal stability of lightweight aggregates. Secondly, its improved insulation properties lead to better thermal conductivity and allow for reduced concrete cover. Lastly, LWC exhibits reduced thermal expansion, which minimizes spalling during fire exposure [12]. The residual strength of normal concrete is notably inferior to that of LWC after fire exposure, indicating a greater degree of damage in the former. This is consistent with the findings of Malhotra [13], who showed that LWC has lower thermal conductivity and a lower coefficient of thermal expansion across all temperature ranges except those relevant to normal-weight concrete. The expansion of aggregates at higher temperatures varies depending on the coefficient of thermal expansion and the cement-to-aggregate ratio. For instance, the coefficient of the thermal expansion of a lightweight expanded clay aggregate (LECA) is approximately 50–70% lower than that of gravel, which has a coefficient of about 12×10^{-6}/K.

Moisture is another critical factor that contributes to the development of vapor pressure, which can cause explosive spalling during the early stages of a fire. The moisture clog theory, developed by Shorter and Harmathy [14], provides insights into the role of moisture. As a concrete specimen is heated, water is released from a thin surface layer. This creates a pressure gradient that forces moisture deeper into the cooler regions of the concrete. As steam encounters cooler layers, it condenses, forming a saturated zone referred to as the "moisture clog". The moisture clog creates a barrier that impedes the movement of steam, building up pressure. When this pressure exceeds the tensile strength of the concrete, spalling occurs, causing parts of the concrete to break off [15].

Moreover, the decrease in compressive strength of LWC after heat treatment is primarily caused by the dehydration of the C-S-H gel and the decomposition of calcium hydroxide. The spread of micro-cracks in the interfacial transition zone, which forms between aggregates pre-saturated with water, may also contribute to this reduction in strength. Reducing

the initial moisture content of lightweight aggregates can help decrease the porosity of the interfacial transition zone, thus enhancing the fire resistance of LWC [16]. In tests conducted at 1000 °C, incipient cracks were observed in LWC, significantly impairing its mechanical properties. Despite visible color changes and the appearance of substantial cracks, the LWC did not experience explosive spalling. However, its compressive strength dropped by more than half compared to its original value under normal conditions [17].

Repairing fire-damaged components requires careful consideration of factors such as the extent of damage, shape of the component, materials used for repair, cost, time, and functional requirements. Although extensive research has been conducted on repairing reinforced concrete structures [18], there remains a lack of funding and focus on restoring buildings damaged by fire. For instance, researchers evaluated the performance of reinforced concrete columns that had been repaired after exposure to high temperatures. Researchers found that in most cases, the repaired columns either returned to their original strength or exceeded that of reference columns in terms of stiffness [19]. In contrast, a study on fire-damaged buildings showed that, with proper repair techniques, demolition could be avoided. Methods such as stiffening, shotcrete repairs, and epoxy injection were successfully used to restore structural integrity [20].

Common methods for repairing damaged concrete components include adding an exterior reinforced concrete support, shotcrete concrete jackets, or attaching metal plates with epoxy. An alternative approach involves using fiber-reinforced composite materials, such as carbon or glass fiber-reinforced polymers, instead of steel plates. These materials offer superior strength-to-weight ratios, durability, toughness, and cost efficiency, making them increasingly popular for the restoration of reinforced concrete components [21,22].

Engineered cementitious composites (ECCs), developed in the early 1990s, are highly ductile materials reinforced with fibers. ECC stands out for its strain-hardening behavior and high ductility, typically ranging from 3 to 7% [23]. With a fracture width of around 60 μm and a fiber content of less than 2%, ECC offers superior control over crack formation [24]. Unlike traditional concrete, ECC behaves more like a metallic material post-cracking due to the micromechanics model that governs the interactions between fibers, the matrix, and the fiber-matrix interface [25].

The unique fracture behavior, tensile strength, and ductility of ECC make it particularly suited for repair applications. Its versatility allows it to be used for trenchless rehabilitation, casting, and spraying. Zhang [26] suggested that using highly ductile ECC as an overlay material can prevent or mitigate the formation of reflective cracks in concrete airport pavements exposed to aircraft loads and environmental stresses. ECC overlays have been shown to significantly enhance the flexural strength, impact resistance, and fatigue durability of airport pavements [27]. The effectiveness of ECC in repairing tension cracks in concrete panels was also demonstrated in a study by Ahmadi et al. [28], who used ECC with fly ash and slag as repair materials. The repaired panels exhibited improved crack resistance and leak prevention due to ECC's strain-hardening and tensile strength properties.

Further research by Kim et al. [29] compared the performance of sprayed ECC and prefabricated mortar as repair materials. ECC displayed superior mechanical properties, including higher strain capacity, better control over crack widths, and higher energy absorption. In summary, ECC has proven to be a highly sustainable and effective material for repair due to its durability and mechanical advantages; however, there is limited research on the use of ECC as a restoration material for fire-damaged concrete structures.

2. Objectives

The aim of this research is to evaluate the effectiveness of an engineered cementitious composite with a basalt fiber-reinforced polymer grid (ECCBFG) in enhancing the structural

performance of fire-damaged LWC T-beams. This study aims to assess the impact of fire exposure on key mechanical properties such as compressive strength, ductility, and load-bearing capacity and to investigate the role of ECCBFG layers in restoring and improving these properties. Additionally, the research seeks to determine the optimal ECCBFG layer thickness required for significant structural improvements under varying fire exposure durations. By comparing the performance of strengthened T-beams with both fire-damaged and undamaged control beams, the study aims to quantify the extent of recovery and enhancement in structural behavior. The findings will provide insights into using advanced composite materials for rehabilitating fire-damaged concrete structures, promoting more resilient and sustainable construction practices.

3. Experimental Work

The experimental program is divided into three main phases. The first phase involves the selection, preparation, and evaluation of raw materials based on their physical and chemical properties. This process includes producing LWC with a target compressive strength of 33 MPa, using LECA for LWC. Once mixed, the T-beam specimens were cast in pre-prepared metal molds and removed after one day. In the second phase, after 28 days of curing, the LWC T-beams and specimens were subjected to fire exposure for 30 and 60 min. This phase involved testing both exposed and unexposed concrete specimens. The third phase consisted of repairing and strengthening the fire-damaged T-beams using a U-shaped ECCBFG layer. The three phases are detailed in the sections that follow.

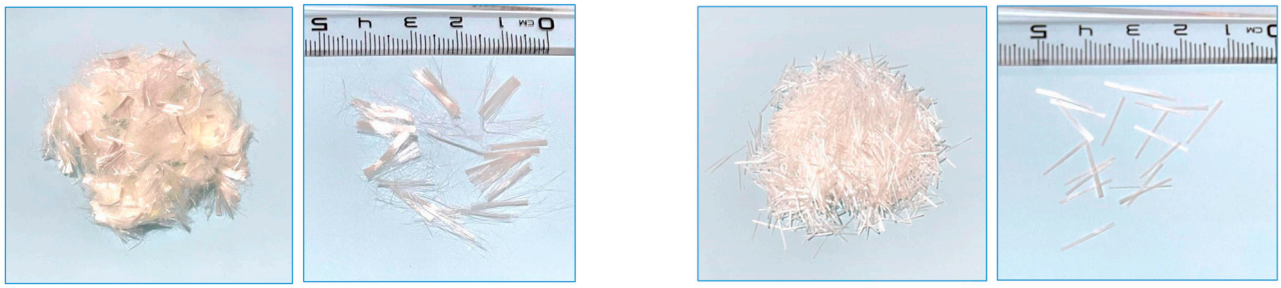
3.1. Material Properties

Fine aggregate (sand) size is critical for ECC, as it must be fine enough to enhance the fluidity of the mixture and ensure uniform fiber dispersion. The sand used had a maximum grain size of 250 μm and a mean size of 110 μm, while the fine aggregate size for LWC of 0.60 mm was used. High-strength LECA was used, with particle sizes ranging between 4.75 and 10 mm. LECA is characterized by porous ceramic materials with uniform, small, closed-cell pores and tightly sintered, strong exterior surfaces. Manufactured from clay minerals, LECA is produced in rotary kilns at temperatures between 1100 °C and 1200 °C, which causes the particles to expand significantly. The LECA used met the ASTM C330 [30] requirements for lightweight aggregates. To reduce water absorption during the mixing process, LECA was submerged in water for at least 48 h. Following this, the aggregate was air-dried under laboratory conditions to achieve a saturated surface dry condition, in line with ACI 211.2-98 [31].

The cement used in this study was ordinary Portland cement, which complied with the standards set by EN 197-1:2011 [32]. GGBS is a granular material produced by rapidly cooling molten iron blast furnace slag with water. It has a minimal crystalline structure and strong cementitious properties. The GGBS used in this study adhered to the specifications of BS EN 15167 [33] and was pulverized to a fine consistency to form hydrates similar to those of Portland cement. Fly ash is a byproduct of coal combustion in thermal power plants, and it is commonly used in concrete production. The fly ash used in this study met the standards of BS 3892 Part 1 [34] and BS EN 450-1:2012 [35]. Classified as Class F fly ash, it had a specific gravity of 2.70 g/cm^3 and a Blaine-specific surface area of 2970 cm^2/g. Also, a high-performance water-reducing admixture was used in this study that complied with ASTM C494/C494M [36]. An admixture dosage of 3.7% by weight of cement was used to achieve the desired slurry consistency for ECC.

Polyvinyl alcohol fibers (PVA) and glass fibers (GFs) were employed to reinforce the ECC, forming a hybrid fiber system. These fibers are known for their strong adhesion to the cement matrix due to the formation of a calcium hydroxide ($Ca(OH)_2$) layer around the

fibers, which enhances bonding strength. A fiber content of 2% by volume was incorporated into the ECC mix. Figure 1a exhibits the PVA employed in this study. The technical parameters of PVA utilized, as reported by the manufacturer company, are presented in Table 1.



(**a**) (**b**)

Figure 1. (**a**) PVA fiber used in this research. (**b**) Geometrical configuration of glass fiber used.

Table 1. Properties of PVA and Glass fibers.

Fiber	Fiber Length (mm)	Diameter (μm)	Tensile Strength (MPa)	Young's Modulus (GPa)	Fiber Elongation (%)	Density (kg/m^3)
PVA	12	29	1600	40	4–10	1.3
GF	12	33	2200	80	0–4	2.78

Glass fibers (GFs) were added to the ECC mix containing PVA fibers, with a fiber volume percentage of 0.5%, forming a hybrid fiber system. The characteristics of the glass fibers are detailed in Table 1, and Figure 1b shows the glass fibers used in this study.

The mesh used was a bidirectional grid made from primed alkali-resistant basalt fiber. Nylon fibers were woven to secure the mesh strands at the intersections along both the warp and weft directions. According to the technical specifications shown in Figure 2, the grid had a nominal cell size of 25.4 × 25.4 mm. The unit weight of the grid was 350 g/m^2, with a fiber density of 2.75 g/cm^3 and an equivalent thickness of 0.38 mm. The manufacturer provided nominal values for the grid's tensile strength, ultimate strain, and Young's modulus, which were 50 kN/m, 1.8%, and 89 GPa, respectively. Table 2 summarizes the mechanical properties of the mesh as provided by the manufacturer.

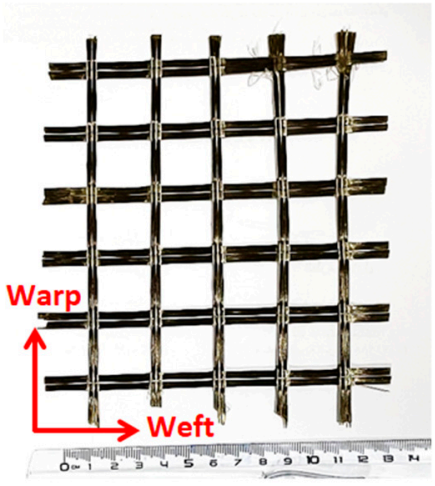


Figure 2. Basalt polymer grid used.

Table 2. Mechanical characteristics of the Basalt mesh.

Material Basalt	Unit Weight (g/m^2)	Mesh Size (mm)	Tensile Strength (KN/m)	Young's Modulus (GPa)	Elongation at Failure (%)	Density (g/cm^3)	Equivalent Thickness (mm)
Fiber Grid	350	25.4 × 25.4	60	89	1.80	2.75	0.38

3.2. Specimen Preparation of LWC

In this study, the T-beams used were 1500 mm in length and constructed from LWC. To reinforce the beams, four deformed steel bars with a diameter of 8 mm were placed at the top, and three deformed steel bars with a diameter of 10 mm were positioned at the bottom. Additionally, 6 mm steel bars were used to strengthen the stirrups, as illustrated in Figure 3. The beams were examined with two different concrete cover thicknesses, 20 and 30 mm.

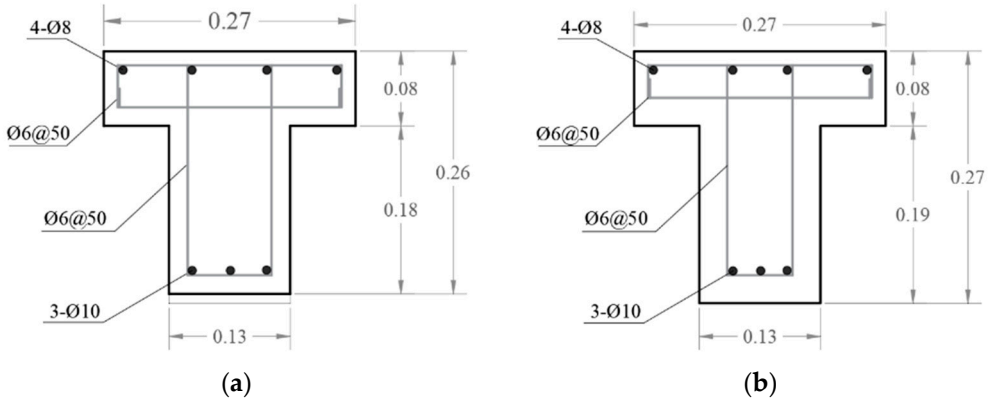


Figure 3. Main section geometry and typical LWC T-beam cross-section (**a**) with 20 mm concrete cover and (**b**) with 30 mm concrete cover.

Table 3 and Figure 4a present the final LWC mix design, which was determined after conducting several rigorous tests. For easier reference, the study assigned specific symbols to each T-beam configuration based on shape and exposure conditions, as shown in Table 4. Each LWC T-beam is identified by four symbols to facilitate the comparison of the different specimens. The first symbol represents the grade of concrete, which in this case is NSC. The second symbol refers to the concrete cover thickness, either 20 or 30 mm. The third symbol denotes the fire exposure duration—30 min, 60 min, or no fire exposure. Finally, the fourth symbol indicates the width of the U-shaped ECC jacket, with values of 0 mm, 20 mm, or 30 mm. The sample recognition system is illustrated in Figure 5.

Table 3. Summary of LWC T-beam details.

Concrete Cover (mm)	ECC Jacket Thickness (mm)	Fire Duration (Min)	Beam Designation
20	None	0	NC2-F0E0
20	None	30	NC2-F1E0
20	None	60	NC2-F2E0
20	20	30	NC2-F1E2
20	20	60	NC2-F2E2
20	30	30	NC2-F1E3
20	30	60	NC2-F2E3
30	None	0	NC3-F0E0
30	None	30	NC3-F1E0
30	None	60	NC3-F2E0
30	20	30	NC3-F1E2
30	20	60	NC3-F2E2
30	30	30	NC3-F1E3
30	30	60	NC3-F2E3

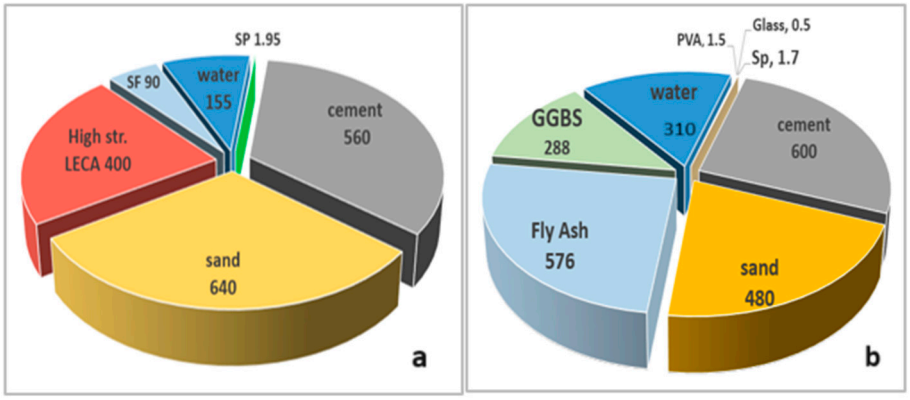


Figure 4. Material proportion of (**a**) LWC and (**b**) ECC mixture.

Table 4. Details of LWC mixes (kg/m^3).

Cement (kg/m^3)	Sand (kg/m^3)	LECA (kg/m^3)	Water (kg/m^3)	SP by wt. of mm (%)	W/Cm	Slump (mm)	Fresh Density (kg/m^3)	28-day Compressive Strength (MPa)
430	700	(LECA) 420	153	15	0.35	90	1625	38.26

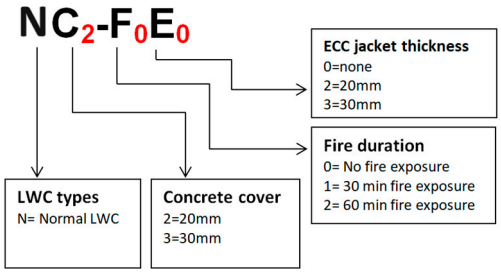


Figure 5. Identifying beams.

Before the casting process, the materials were carefully selected and measured according to the volume requirements of the mixture. In this investigation, all T-beams were fabricated using metal molds, as shown in Figure 6, which illustrates the casting process for reinforced LWC T-beams. Table 5 and Figure 4b present the optimal material combinations used in this study, along with their corresponding weight proportions, which were determined after conducting multiple experimental trials. The optimal ECC mixture, which exhibited excellent workability, flow, and homogeneity, was achieved by combining fly ash and GGBS in a ratio of 0.8 (fly ash) to 0.4 (GGBS), along with hybrid fibers consisting of 1.5% PVA fibers and 0.5% glass fibers. The process of optimizing the ECC mixture began with the selection of components based on compatibility and prior research, followed by preliminary mix trials to evaluate workability, flowability, and homogeneity. Each mix underwent mechanical testing to assess compressive strength, tensile strength, and ductility, and the mix meeting the target criteria was shortlisted. Further optimization was performed by adjusting the ratios of fly ash to GGBS (0.8:0.4) and the fiber content (1.5% PVA fibers and 0.5% glass fibers) to achieve a balance between mechanical performance and cost-effectiveness. The final mix was selected based on its superior strength, ductility, and flowability, and this process is now detailed in the revised manuscript to enhance clarity and transparency.



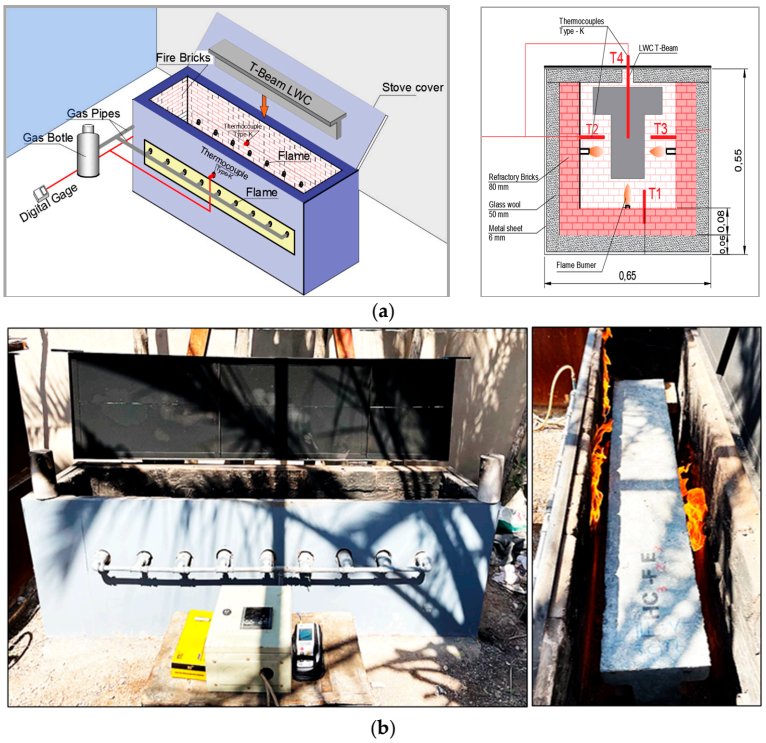
Figure 6. Processes of casting LWC T-beam specimen.

Table 5. Material mix proportion of ECC.

Cement (kg/m^3)	Sand (kg/m^3)	Fly Ash (kg/m^3)	PVA Fiber Vol.%	Glass Fiber Vol.%	W/B Ratio	Water (kg/m^3)	Super Plasticizer by wt. of Cement (%)
600	480	720	1.5	0.5	0.23	310	1.7

3.3. Applying Elevated Temperature on LWC Beams

A brick furnace was constructed locally to expose the concrete T-beams to elevated temperatures. The furnace was equipped with thermocouple sensors and a portable data-gathering system to monitor and record temperature changes over time, as shown in Figure 7. After 56 days of curing, the LWC T-beams were subjected to fire in the furnace. The heating process followed the ISO-834 [9] standard fire curve, depicted in Figure 8, with the furnace designed to reach a peak temperature of 1200 °C. The temperature inside the furnace was controlled according to the ISO-834 [9] curve, and the rate of heating closely adhered to the standard guidelines.



(**a**)

(**b**)

Figure 7. (**a**) Details and section of furnace and equipment. (**b**) Burning furnace with all connections.

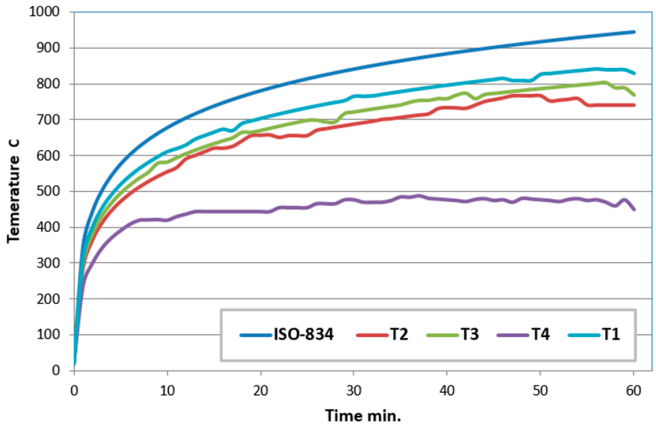


Figure 8. Experimental and ISO-834 [9] standard recommended temperature–time curves.

Each fire-loading session lasted 30 min or 1 h, which was sufficient to raise the temperature of the LWC T-beams to the desired level. Observations were made every 5 min using viewports in the furnace to detect any significant changes in the specimens, such as fire-induced spelling. Once the fire exposure was completed, the T-beams were allowed to cool to ambient temperature (approximately 35 °C). A thorough evaluation was then conducted to assess the severity of cracks and spalling. The beams were cooled further after removal from the furnace to ensure that they were ready for the post-fire analysis. The heating rate during fire exposure of T-beams in the furnace closely followed the ISO-834 [9] guideline curve, with only a minor deviation of around 11% during the 60-min exposure period.

3.4. Repairing Damaged LWC Beams with ECC Jackets

A modern method for strengthening reinforced concrete structures involves the use of thin jackets made from ECCBFG. These materials exhibit excellent compressive strength and strain-hardening behavior under tension, eliminating the need for traditional reinforcement elements like rebar or stirrups. In this experiment, the ECCBFG was found to be the most effective method for creating the ECCBFG thin jacket, applied at thicknesses of 20 and 30 mm. The mechanical behavior of the matrix and material composition were thoroughly investigated.

The thin ECCBFG jackets were applied to fire-damaged LWC T-beams to restore the three damaged sides of each beam. The jackets, U-shaped in design, were constructed using a basalt fiber-reinforced polymer grid. A specially designed metal mold, extendable to 20 and 30 mm, was used to cast the ECC jackets. The basalt grid was secured with epoxy–plastic connectors at several points along the three sides of the T-beam, ensuring that it was centrally positioned within the repair layer before the ECC was poured. During the casting process, careful monitoring ensured that the ECC penetrated the basalt fiber grid evenly, achieving a leak-free and homogeneous distribution throughout the jacket. Figure 9 illustrates this process.

After fire exposure, the damaged beams, which showed cracks and flaking, were repaired before strengthening using the ECCBFG jacket. The repair process involved four key steps, as shown in Figure 10. First, specialized equipment was used to remove the damaged, charred, and fragile areas, followed by thorough cleaning with water and compressed air to eliminate dust and debris. Second, grooves were cut at approximately 45-degree angles using hard stone cutting disks to create a rough surface, ensuring a strong bond between the concrete beam and the ECCBFG jacket. Third, the basalt fiber-reinforced polymer grid was secured to the sides, and bottom of the beam using epoxy–plastic connectors, and spacers were placed along the bottom and sides to maintain the jacket's thickness. Lastly, the ECC material, known for its excellent flowability, was injected

gradually into the mold without the need for vibration, ensuring even coverage of the gaps and a uniform jacket thickness of 2 or 3 cm. This process was carried out after the mold was properly cleaned and the spacers were secured to achieve the desired jacket dimensions.

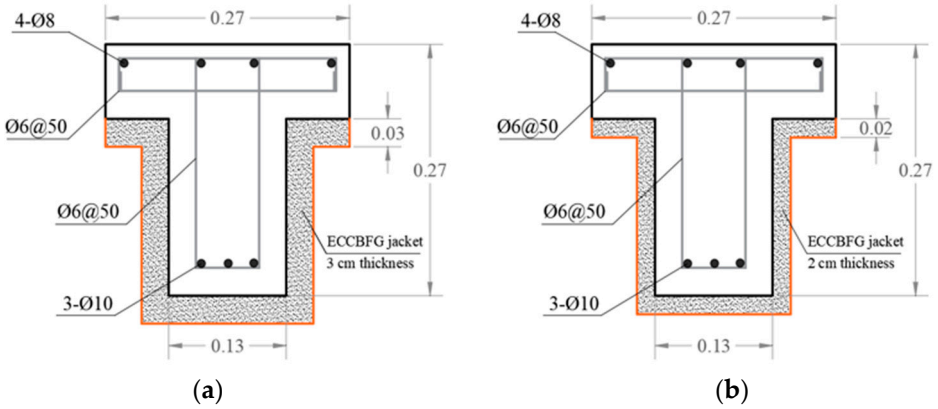


Figure 9. Strengthened section using three-face ECCBFG jacket (**a**) with 30 mm cover, and (**b**) with 20 mm cover.

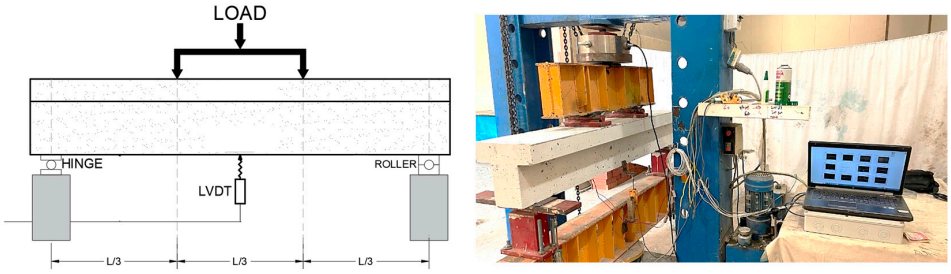


Figure 10. Garment processes of strengthening LWC beam specimen.

3.5. Testing Procedure

After casting, all repaired LWC T-beams were cleaned and coated with white emulsion paint to facilitate crack observation during testing and improve the visibility of fracture propagation. The horizontal alignment of each T-beam was confirmed prior to testing by using a spirit level to check both sides. A four-point loading method was employed to

evaluate the flexural performance of the T-beams, as shown in Figure 11. This method creates a pure bending area across the T-beam, ensuring consistent load distribution and moment failure.



(**a**) (**b**)

Figure 11. (**a**) Loading setup and measurements. (**b**) Arrangement of LVDTs and load cell within test device.

As shown in Figure 11, the end supports of the T-beams were spaced 1.35 m apart. A steel beam was used to apply the load, which was distributed at two points along the length of the T-beam, simulating an equally distributed load across the beam. The two-point loads were positioned 0.45 m apart. A 600 kN hydraulic testing machine, operating under stroke control, applied stress to the T-beams at a rate of 0.02 kN/s. Each T-beam was tested under a monotonically increasing load until failure occurred, as depicted in Figure 11.

The load application was monitored using the machine's load cell, while the actuator displacement and LVDT (Linear Variable Differential Transformer) were used to measure deflection at the midpoint of the beams. The testing was conducted in the laboratory at the University of Babylon, College of Engineering. All LWC T-beams were tested over a 28-day period under increasing stress until failure, using calibrated electro-hydraulic testing equipment.

4. Results and Discussion

This section presents a detailed analysis of the data obtained from the experimental laboratory program. The study aims to compare the effects of different fire exposure durations (30 and 60 min), concrete cover thicknesses (20 and 30 mm), and varying ECCBFG jacket thicknesses (20 and 30 mm) on several performance indices. These indices include the load-carrying capacity, cracking load, mid-span displacement at maximum load, energy absorption, and ductility index.

4.1. Load–Displacement Behavior

All load–displacement curves exhibited elastic behavior before the beams reached their breaking points. After failure, beams reinforced with ECCBFG demonstrated varying behavior patterns. As shown in Figures 12 and 13, the ultimate load-carrying capacity of LWC T-beams decreased significantly after 60 min of fire exposure. The deterioration rates were 28.6% for beams with a 20 mm concrete cover and 21.7% for those with a 30 mm cover. The load–deflection behavior observed after 30 and 60 min of fire exposure showed a noticeable decline compared to the reference specimens. The NC2-F1E0 and NC2-F2E0 T-beams exhibited primarily linear behavior up to the ultimate load, with minimal hardening and limited ductility. In contrast, the NC3-F1E0 demonstrated better performance, sustaining a higher load at greater displacements than the NC3-F2E0.

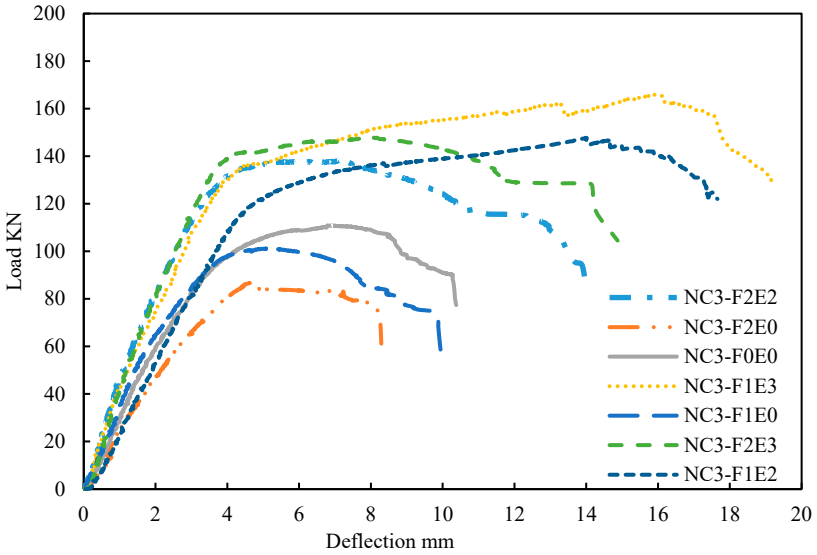


Figure 12. Load–deflection at mid-span curve of LWC T-beam specimen with concrete cover (30 mm) before and after fire exposure.

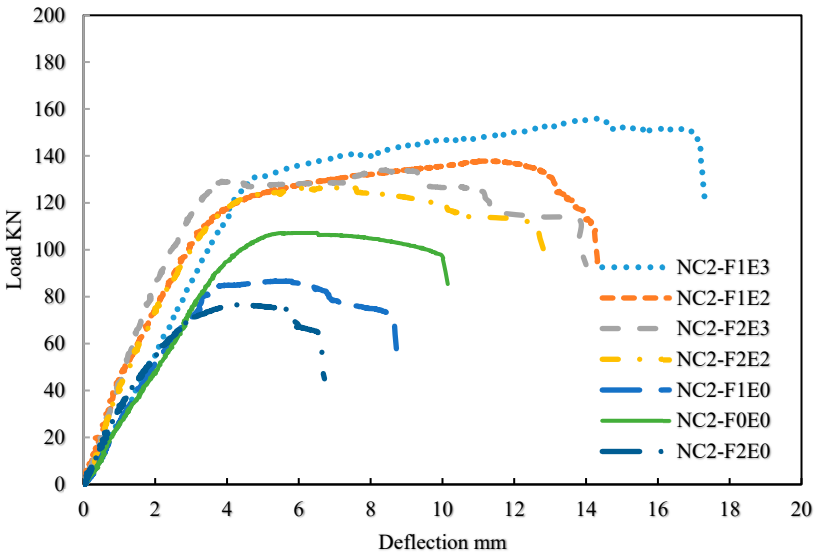


Figure 13. Load–deflection at mid-span curve of LWC T-beam specimen with concrete cover (20 mm) before and after fire exposure.

Increasing the concrete cover from 20 to 30 mm reduced the deterioration in ultimate load capacity due to fire exposure by 10.2% and 7.0%, respectively, for fire exposure durations of 30 and 60 min without strengthening. Strengthening with ECCBFG jackets improved load capacity by 4.6% to 5.0% for ECC jacket thicknesses after 30 min of fire exposure. Figure 12 shows that the load-carrying capacity of beams reinforced with ECCBFG increased by 7.0% to 9.0% after 60 min of fire exposure. The strengthened T-beams (NC3-F1E3) showed a 150% increase in load capacity, nearly linear behavior up to failure, strong ductility, and high energy absorption after 30 min of fire exposure. Additionally, NC3-F1E3 exhibited higher load capacity than NC3-F1E2. After 60 min of fire exposure, the NC3-F2E3 specimen, with a 30 mm ECCBFG jacket, outperformed the NC3-F2E2 specimen, which had a 20 mm jacket, in terms of load capacity and ductility. Figure 12 also highlights that the ductility of the T-beams (NC3-F1E3 and NC3-F1E2) improved after strengthening with ECCBFG. The four-point bending test proved to be an effective method for indirectly evaluating ECC's strain-hardening ability, as previously noted by Yuan et al. [37].

Table 6 summarizes the results of the T-beam testing for LWC beams with concrete cover thicknesses of 20 and 30 mm. The table includes key measurements such as the load at which initial cracking occurred, the load at failure, maximum deflection at mid-span, and the residual load after failure. The load-carrying capacity of the T-beams was assessed using these parameters, with the fracture pattern serving as an early indicator of stress response. The progression of fractures as they developed under increasing load was closely observed, providing valuable insight into the beams' structural performance and failure behavior.

Table 6. Results of LWC T-beams.

T-Beam Description	First Crack Load, KN	Ultimate Load, KN	Percentage Residual Ultimate Load, %	Max Deflection (mm) At Mid-Span
NC2-F0E0	21.22	107.30	100	6.77
NC2-F1E0	16.51	86.62	80.7	5.40
NC2-F2E0	11.70	76.59	71.3	4.00
NC2-F1E2	42.20	138.02	128.6	9.20
NC2-F1E3	71.33	155.89	145.2	14.60
NC2-F2E2	32.90	126.49	117.8	7.65
NC2-F2E3	58.41	133.94	124.8	11.00
NC3-F0E0	22.52	110.83	100	7.00
NC3-F1E0	19.14	101.11	91.2	5.21
NC3-F2E0	15.20	86.71	78.2	4.60
NC3-F1E2	45.70	147.69	133.2	13.98
NC3-F1E3	73.30	165.97	150.0	15.96
NC3-F2E2	40.80	138.22	124.7	7.38
NC3-F2E3	60.40	147.77	133.3	8.20

The other criterion for evaluating the structural behavior of the T-beam specimens with a 30 mm concrete cover is the load-carrying capacity with varying ECCBFG jacket thicknesses. The results can then be compared to T-beams with a 20 mm concrete cover. Figure 14 presents these comparisons. The load-carrying capacity of the reference T-beams before fire exposure was nearly identical for both 20 and 30 mm concrete covers, as the T-beams had the same effective depth regardless of the cover thickness. The load-carrying capacities for 20 and 30 mm covers were 107.30 kN and 110.83 kN, respectively.

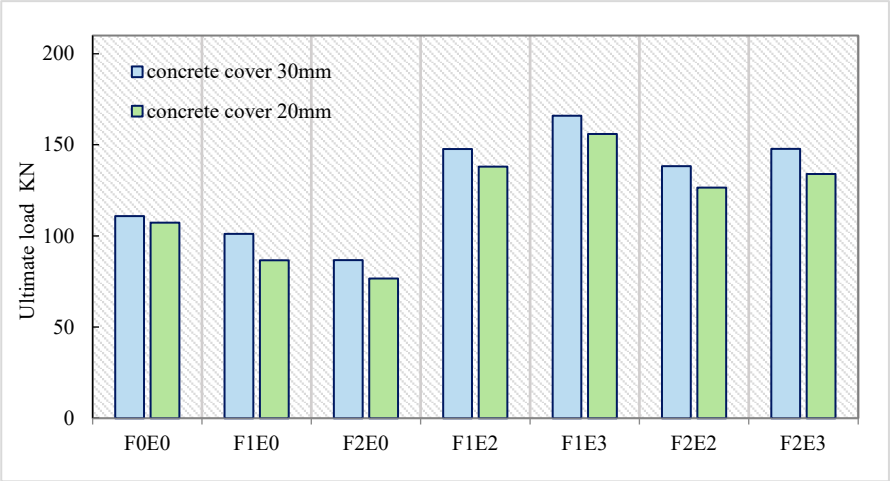


Figure 14. Influence of concrete cover (30 and 20 mm) on LWC T-beam load-carrying capacity.

T-beams with a thicker concrete cover experienced less loss of load-carrying capacity after fire exposure, as the larger cover provided better protection for the effective concrete section and reinforced steel from fire damage. Figure 15 shows that the reduction in load capacity was 9.0% for a 30 min fire exposure and 21.0% for a 60 min exposure with a 30 mm concrete cover. In contrast, for T-beams with a 20 mm concrete cover, the reduction

was significantly higher, with a 19.0% decrease after 30 min of fire exposure and a 28.0% decrease after 60 min.

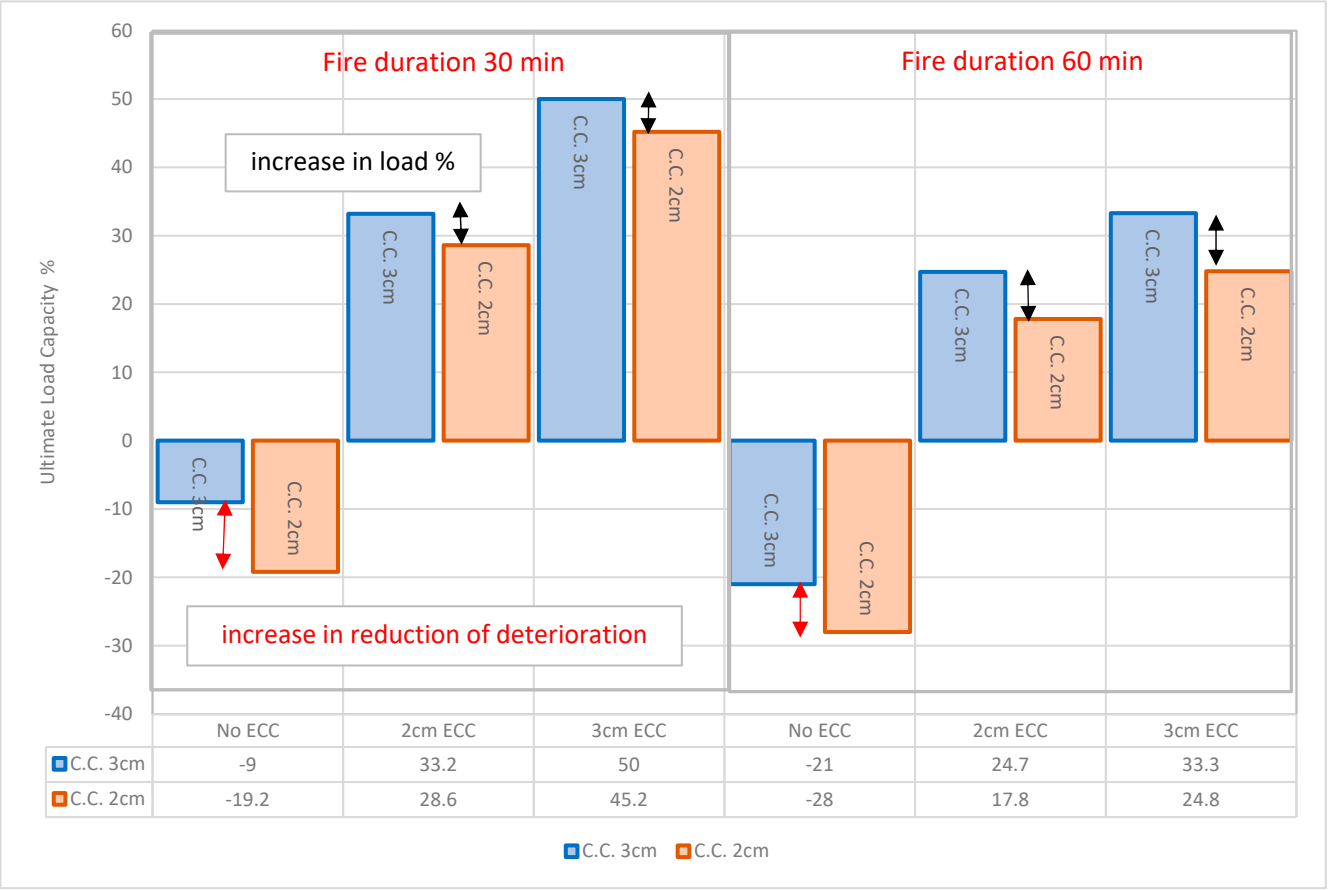


Figure 15. The percentage of the load-carrying capacity of LWC T-beam specimen's exposure to fire with different concrete covers.

The results indicated that the 30 mm concrete cover remained largely intact for the T-beams exposed to fire and reinforced with the ECCBFG. The load-carrying capacity improved by approximately 32% and 25% after 30 and 60 min of fire exposure, respectively, when a 20 mm thick ECCBFG jacket was applied. Similarly, for T-beams reinforced with a 30 mm thick ECCBFG jacket, the load-carrying capacity increased by 50% and 33% after 30 and 60 min of fire exposure, respectively.

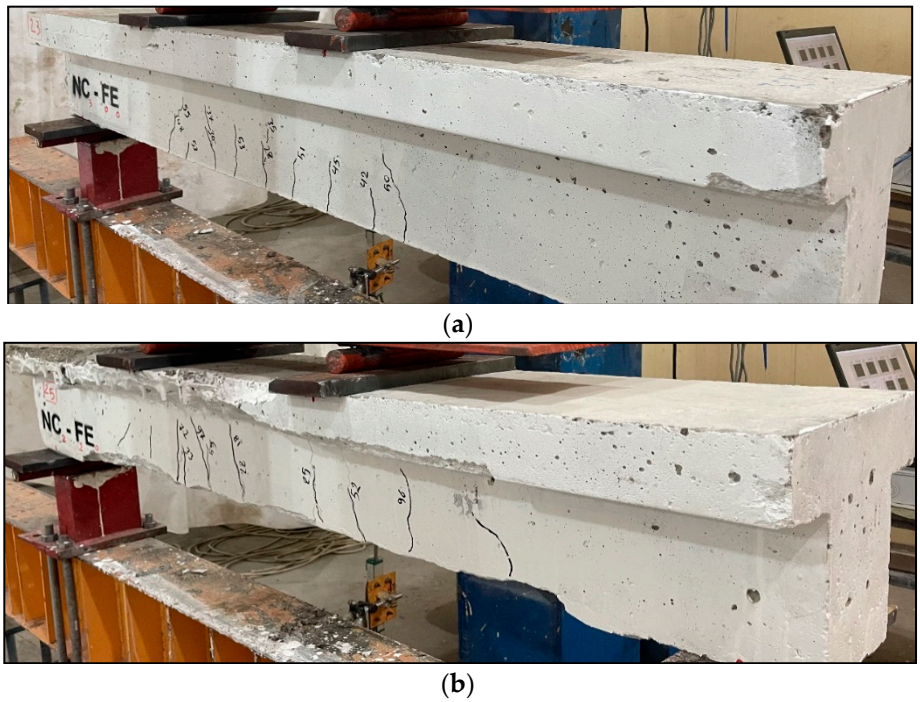
4.2. Crack Patterns and Failure Modes

After fire exposure, the T-beams exhibited pale gray surfaces with reddish spots indicative of fire damage. As shown in Figure 16, microscopic reticular fractures were observed on the exposed surfaces. After 1 h of exposure to high temperatures, random cracks measuring between 0.05 and 0.19 mm developed across the concrete surface. These surface cracks were most pronounced around the main and transverse reinforcing points, where the expansion of the reinforced concrete elements created significant tensile stresses. The differential thermal expansion of the cement matrix and aggregates likely contributed to these fractures. Additionally, the beams experienced concrete spalling to a depth of up to 15 mm. Despite the fire damage, the beams had no visible curvature, indicating that the overall structural geometry remained largely intact.



Figure 16. Hairline-cracked fired-exposed T-beam.

As shown in Figure 17, flexural cracks were spaced out across the mid-span region in both the reference beam and fire-damaged beams without repairs. Similar crack patterns emerged as stress increased in both the reference and damaged beams. While the reference beam developed new flexural cracks under stress, the fire-damaged beams extended their pre-existing cracks. In both the reference and fire-damaged beams with 20 and 30 mm concrete covers, the first crack appeared around the mid-span region. The reduction in cracking load for fire-exposed beams may be attributed to the weakened reinforcing steel at high temperatures.



(**a**)

(**b**)

Figure 17. (**a**) Crack pattern of LWC T-beams before burning. (**b**) Crack pattern of LWC T-beams after fire exposure.

Although the T-beams had different concrete coverings, the failure modes of NC2-F0E0 were similar to those of NC3-F0E0. As shown in Figure 18, NC3-F0E0 exhibited fewer cracks and less expansion compared to the other method. After the fire exposure, one main

crack became more prominent, and crack patterns on both sides of the beam appeared almost identical. Additionally, secondary cracks formed close to one another following the fire. Fire-exposed beams experienced rapid bending, likely due to the reduction in concrete strength. Furthermore, the fire-damaged T-beams developed shear cracks after the formation of flexural cracks. Figure 19 demonstrates that fire exposure reduces the shear strength of concrete, which may explain this behavior.

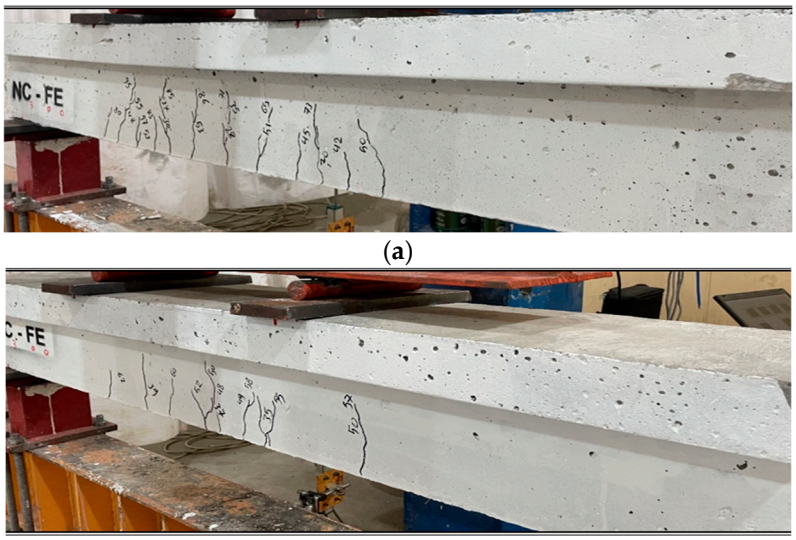


Figure 18. Crack pattern of LWC T-beams before fire exposure. (**a**) Concrete cover, 20 mm; (**b**) concrete cover, 30 mm.



Figure 19. Shear crack pattern of LWC T-beams after fire exposure.

The T-beams reinforced with the ECCBFG jacket exhibited increased deflection, characterized by deflection-hardening behavior and significant flexural deformation. The fracture width was effectively controlled within a limited range, owing to the crack-bridging capabilities of PVA fibers and the basalt grid, as shown in Figure 20. This crack control was achieved by combining the inhibitory effects of crack propagation from both materials. Once the T-beams reached their maximum bending strength, they demonstrated deflection-softening behavior, with the load systematically decreasing as deflection increased. At this point, the PVA fibers and basalt grid began to displace, either being pushed out or peeled off, resulting in further deformation. As a result, the fibers and grid were no longer able to prevent the propagation of initial cracks on the surface. The appearance of multiple minor fractures eventually led to the propagation of major cracks, as the crack pattern in the pure bending area of the ECCBFG-reinforced T-beams evolved.



(**a**)



(**b**)

Figure 20. Fine multiple cracks of LWC T-beams strengthened with (**a**) 3 cm ECCBFG and (**b**) 2 cm ECCBFG.

4.3. Absorption Energy

The area under the load-deflection curve represents the energy absorbed by the reinforced concrete beams. Energy absorption before the maximum load refers to the total energy a beam can absorb before its load-bearing capacity begins to decline significantly. This is depicted by the area enclosed by the curve from the start to the peak load, as noted by Deng and Zhang [38]. Reinforced concrete members inherently possess ductility and energy absorption capabilities, allowing them to convert mechanical energy into internal potential energy due to their intrinsic malleability.

The process of energy absorption In concrete materials Involves both elastic and plastic deformations, particularly during cracking. When reinforced concrete members are strengthened with various materials, their energy absorption capacity becomes a critical structural property, as highlighted by Lee et al. [39]. This attribute plays a key role in enhancing the overall performance and resilience of reinforced concrete structures.

Since fire reduces the load-carrying capacity of T-beams, the energy absorption capacity is based on the area under each T-beam's load-displacement curve, providing a more accurate measure of ductility. The energy absorption capacity of concrete structures is a crucial indicator of their ability to withstand natural and man-made disasters such as earthquakes, fires, and terrorist bombings. Table 7 and Figure 21 present the energy absorption data for LWC T-beams measured both before and after fire exposure.

Fire reduced the energy absorption of LWC T-beams. After 30 min of fire exposure, LWC T-beams with concrete cover (20 and 30 mm) absorbed 26.9% and 24.4% less energy. However, the same cover's one-hour exposure decreased by 51.9% and 42.3%, showing a greater reduction. Fire causes LWC T-beams' load–displacement curves to rise less steeply and linearly, then drop rapidly before collapsing. This may be because energy absorption computations depend only on beam displacement. Concrete loses its energy-absorbing ability after extended fire exposure and cracks. This reduction in energy absorption may be due to mechanical deterioration in concrete and steel. The reinforcing bars' adherence to the concrete decreased as the temperature rose. The decreasing bonding strength suggests that the reinforcing bars were not strong enough.

Table 7. Energy absorption capacity and residual energy absorption of LWC T-beams.

T-Beam Description	Energy Absorption, kN.mm	Increasing or Decreasing Energy Absorption, %
NC2-F0E0	540.13	-
NC2-F1E0	408.07	−24.4
NC2-F2E0	311.21	−0.423
NC2-F1E2	1669.08	+209.0
NC2-F1E3	2130.23	+294.3
NC2-F2E2	780.35	+44.4
NC2-F2E3	1100.80	+103.8
NC3-F0E0	495.88	-
NC3-F1E0	362.36	−26.9
NC3-F2E0	238.20	−51.9
NC3-F1E2	1199.52	+141.8
NC3-F1E3	1790.37	+261.0
NC3-F2E2	626.20	+26.3
NC3-F2E3	912.13	+83.9

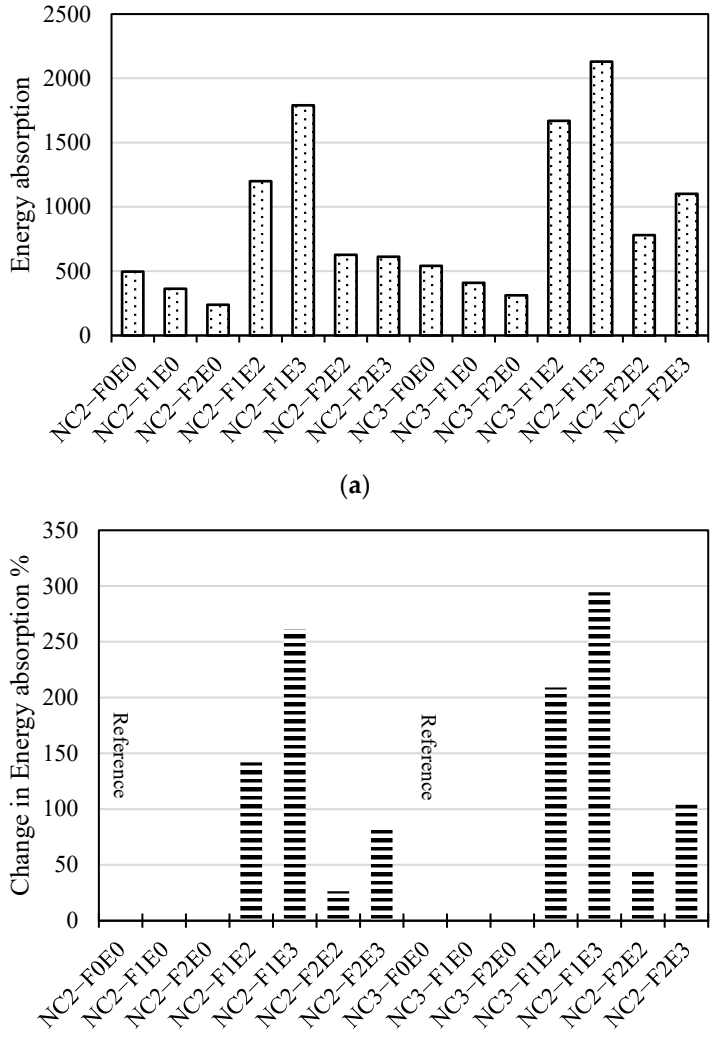


Figure 21. (**a**) Energy absorption of LWC with different fire exposure durations and concrete cover and (**b**) percentage change in energy absorption.

Further investigation revealed that the concrete cover significantly affected energy absorption. After 30 and 60 min of fire exposure, LWC T-beams with larger concrete cover (30 mm) had 11.2% and 23.4% higher energy absorption than those with 20 mm. According

to Table 7 and Figure 21, concrete T-beams strengthened with ECCBFG with a thickness of 20 or 30 mm increase LWC energy absorption significantly. All T-beams strengthened with ECCBFG layers could bear loads and absorb energy more than the control beams. Figure 21 shows that T-beams with an ECCBFG strengthening layer, such as NC3-F1E3, NC3-F1E2, NC3-F2E2, and NC3-F2E3, dissipate 294%, 209%, 103.7%, and 44.4% more energy than reference specimens with concrete covers of 30 mm. This is possibly because the basalt grid in ECC does not break immediately when the sample cracks and still provides tensile strength and energy consumption. More importantly, PVA and glass fibers link the ECC matrix and increase its deformation ability. Strong T-beams with an ECCBFG layer and a concrete cover (20 mm) showed comparable behavior, although the impact was less substantial than with a concrete cover (30 mm). The NC3-F1E3 and NC2-F1E3 T-beams had the highest energy absorption values. Compared to the control beam, the growth ratio was 294% and 260%. LWC T-beams reinforced with 30 mm showed these findings.

The beams featuring a basalt grid, namely NC3-F1E3 and NC2-F1E3, exhibit superior energy absorption compared to the reference and other strengthened T-beams. This is shown by the presence of the basalt grid and fibers (PVA and glass fiber) in these beams. Once the ECC matrix is fractured, the basalt grid can maintain a substantial portion of its resistance to tension. In addition, the PVA fiber was retrieved intact from the material without any fractures occurring during the breaking process. Consequently, the PVA fiber can demonstrate a bonding effect in the matrix, leading to the dispersion of tensile energy throughout the specimen's cracking process.

In addition, it is seen that the energy absorption of T-beams increases when the degree of damage is low after being exposed to fire for 30 min, despite the thickness of the strengthening layer ECCBFG being 20 mm. For instance, the T-beam specimen (NC3-F1E2) exhibited a 209% increase in energy absorption during testing. When the fire exposure duration was extended to 60 min, the T-beam specimen (NC3-F2E3) only showed a modest increase of 103.8%.

Fire significantly reduced the energy absorption capacity of LWC T-beams. After 30 min of fire exposure, LWC T-beams with concrete covers of 20 and 30 mm absorbed 26.9% and 24.4% less energy, respectively. However, after 60 min of exposure, the reduction was more severe, with a 51.9% decrease for the 20 mm cover and 42.3% for the 30 mm cover. Fire exposure altered the load–displacement curves, causing them to rise less steeply and linearly, followed by a rapid drop before failure. This behavior may be attributed to the fact that energy absorption calculations depend on beam displacement. As fire exposure extends, concrete loses its energy-absorbing ability due to the development of cracks and mechanical degradation of both the concrete and steel reinforcement. The weakening bond between the reinforcing bars and concrete at elevated temperatures further contributed to the reduction in energy absorption, as the reinforcing bars lost strength.

A further analysis revealed that concrete cover thickness significantly influenced energy absorption. After 30 and 60 min of fire exposure, LWC T-beams with a 30 mm concrete cover had 11.2% and 23.4% higher energy absorption than those with a 20 mm cover. According to Table 7 and Figure 21, LWC T-beams strengthened with ECCBFG layers (20 or 30 mm thick) demonstrated a significant increase in energy absorption compared to un-strengthened beams. All ECCBFG-reinforced beams exhibited superior load-bearing capacity and energy absorption relative to the control beams. Figure 21 shows that T-beams with ECCBFG layers, such as NC3-F1E3, NC3-F1E2, NC3-F2E2, and NC3-F2E3, absorbed 294%, 209%, 103.7%, and 44.4% more energy, respectively, than reference beams with a 30 mm concrete cover. This improvement is likely due to the basalt grid in the ECC, which does not immediately fracture upon cracking and continues to provide tensile strength and

absorb energy. Additionally, PVA and glass fibers enhance the deformation capacity of the ECC matrix, further improving energy absorption.

Moreover, energy absorption increased when the degree of damage was lower after 30 min of fire exposure, regardless of the ECCBFG jacket thickness. For example, the NC3-F1E2 T-beam exhibited a 209% increase in energy absorption during testing. However, when the fire exposure duration was extended to 60 min, the NC3-F2E3 T-beam showed a more modest increase of 103.8%.

4.4. Ductility

In conventional reinforced concrete structural design, concrete compressive strength is typically considered the most critical requirement. Many assume that material strength directly correlates with structural strength and performance. However, this assumption holds true only when material strength determines the failure mode. In reality, tensile fractures can weaken materials, and using ductile materials like ECC may enhance structural strength and performance instead [40].

Ductility refers to the capacity of reinforced concrete components to undergo inelastic deformation up to failure without a significant reduction in load-carrying capacity. It is measured as the ratio of deformations at the ultimate stage to those at the yield stage. These deformations include deflections, curvatures, and stresses [41]. In this study, the ductility index is defined as the product of the yield deflection and ultimate load deflection of the corresponding elastoplastic system. The deflection values provided in Table 8 can be directly used to calculate the ductility. The ductility calculation is determined using the following formula:

$$\mu = \Delta u / \Delta y \quad (1)$$

where μ is the ductility index. Δu represents the maximal deformation at failure. Δy is the deformation as a result of material yielding. Δy is found from the load-deflection curves through the intersection point of the curve tangent lines, where Δy represents the deflection opposite this point.

Table 8. Ductility Index for NLWC T-beam before and after exposure to fire flame.

T-Beam Description	Yield Deflection Δy in mm	Ultimate Deflection Δu in mm	Ductility Index, $\mu = \Delta u/\Delta y$
NC2-F0E0	3.75	7.00	1.86
NC2-F1E0	3.10	5.21	1.68
NC2-F2E0	3.45	4.60	1.33
NC2-F1E2	4.20	13.98	3.33
NC2-F1E3	3.81	15.96	4.18
NC2-F2E2	3.75	7.38	1.97
NC2-F2E3	3.45	8.20	2.37
NC3-F0E0	3.70	6.77	1.82
NC3-F1E0	3.71	5.40	1.45
NC3-F2E0	3.25	4.00	1.23
NC3-F1E2	3.05	9.20	3.01
NC3-F1E3	4.11	14.60	3.55
NC3-F2E2	3.45	7.65	2.21
NC3-F2E3	3.82	11.00	2.87

Fire significantly reduced the ductility index of LWC T-beams. After 30 min of fire exposure, the ductility index of LWC T-beams with 30 and 20 mm concrete covers decreased by 9.6% and 20.3%, respectively. Following one hour of fire exposure, the reduction in ductility was even more pronounced, with decreases of 28.5% for the 30 mm cover and 32.4% for the 20 mm cover. The load–displacement curves for fire-exposed LWC T-beams exhibited a less steep and linear ascending portion, followed by a rapid descending section

before collapse. This behavior, primarily influenced by beam displacement, may explain the decrease in the ductility index. Prolonged fire exposure causes concrete to lose its ductility, likely due to the mechanical degradation of both the concrete and reinforcing steel. As temperatures increased, the bond strength between the reinforcing bars and concrete weakened, preventing the bars from developing sufficient strength to maintain the bond.

Further investigation revealed that the thickness of the concrete cover had a significant effect on the ductility index. As shown in Figure 22, after 30 min of fire exposure, increasing the concrete cover from 20 to 30 mm resulted in a 15.8% increase in the ductility index. After 60 min of fire exposure, this increase was 8.1%.

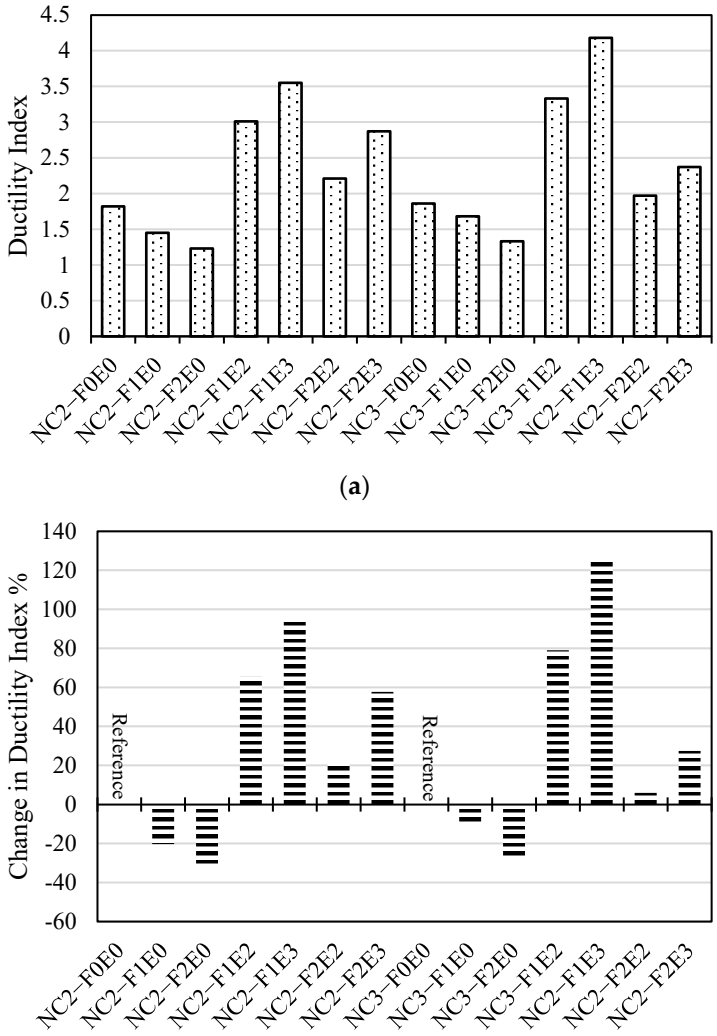


Figure 22. (**a**) Ductility index of NLWC with different fire exposure duration and concrete cover and (**b**) percentage change in ductility index.

As shown in Table 8 and Figure 22, the use of ECCBFG strengthening layers with thicknesses of 20 and 30 mm resulted in a significant improvement in the ductility index for LWC T-beams. The typical cause of failure in these T-beams was flexural cracking on the tension side. T-beams strengthened with ECCBFG layers were able to bear higher loads compared to the control beams. Specifically, when a 30 mm thick ECCBFG layer was applied to LWC T-beams, the ductility index of specimens NC3-F1E3 and NC2-F1E3

was 120% and 95% higher, respectively, than that of the control beam, as demonstrated in Figure 22.

The ductility index tended to increase more significantly when the degree of damage was lower after a 30 min fire exposure, even with a 20 mm ECCBFG strengthening layer. For instance, the T-beam specimen NC3-F1E2 exhibited a 79% increase in ductility, while NC3-F2E3 showed only a 27% increase after 60 min of fire exposure, likely due to the more substantial damage caused by the longer exposure time.

T-beams strengthened with the ECCBFG layer demonstrated the highest deflection capacity and, consequently, the greatest ductility for LWC. This improvement in deflection capacity and ductility can be attributed, in part, to the inclusion of Class F fly ash with GGBS. The combination of fly ash and GGBS reduces the chemical bond between the PVA fibers and the matrix, decreasing matrix toughness. However, it enhances the frictional connection between the fibers and the matrix, allowing the material to withstand higher tensile strain [42,43]. Additionally, the inclusion of the basalt grid in the ECC strengthening layer further enhances strain hardening and increases the material's overall ductility.

5. Conclusions

This research analyzed the effectiveness of a three-sided ECCBFG jacketing layer in improving the performance of fire-damaged LECA LWC T-beams. Key variables included the thickness of the ECCBFG layer, fire exposure duration, and concrete cover thickness. Based on the findings, the following conclusions were reached:

1. Fire exposure significantly reduced the performance of T-beams, with cracking loads decreasing by 32% to 45% and maximum load capacities reducing by 28% and 21% for 20 and 30 mm covers, respectively, after one hour of fire exposure.
2. Strengthening T-beams with ECCBFG jackets substantially enhanced their load capacity. Improvements ranged from 65% to 75% for 20 mm covers and 59% to 70% for 30 mm covers after 60 min of fire exposure. Strengthened T-beams approached the performance of undamaged reference beams.
3. ECCBFG reinforcement significantly improved ductility. Strengthened beams with 30 mm jackets exhibited 120% higher ductility indices than control beams, while those with 20 mm jackets showed a 95% improvement.
4. Energy absorption was reduced by fire exposure, with decreases of 26.9% and 24.4% after 30 min and 51.9% and 42.3% after one hour for 20 and 30 mm covers, respectively. Beams with 30 mm covers retained higher energy absorption than those with 20 mm covers.
5. ECCBFG-reinforced T-beams demonstrated significant energy absorption increases, ranging from 44.4% to 294%, depending on the jacket thickness and fire exposure duration. This improvement is attributed to the tensile resistance and energy dissipation capabilities of the basalt grid and fibers.
6. The inclusion of the basalt grid and PVA fibers enhanced both energy absorption and ductility by providing tensile strength and effective bonding during cracking. These properties made ECCBFG layers an effective solution for rehabilitating fire-damaged T-beams.

While this study demonstrates the effectiveness of ECCBFG in rehabilitating fire-damaged LWC T-beams, further investigations are needed to expand its applicability to real-world scenarios. Future research should explore the long-term performance of ECCBFG-repaired beams under sustained loading, environmental stresses, and cyclic fatigue to assess durability and resilience. Additionally, incorporating computational simulations to model complex fire scenarios, including uneven heat fluxes and flame exposure, will complement experimental findings and provide deeper insights. Comparative analyses with other advanced repair materials, such as CFRPs and GFRPs, should also be conducted to evaluate economic feasibility, material costs, and implementation complexities. Finally,

microstructural studies using advanced microscopy techniques and computational modeling of microfiber effects on mechanical performance and energy dissipation will further enhance our understanding of ECCBFG's potential as a robust rehabilitation material.

Author Contributions: Data curation, H.M.A.-B.; formal analysis, H.M.A.-B. and M.M.K.; investigation, H.M.A.-B.; methodology, H.M.A.-B. and M.M.K.; project administration, M.M.K.; resources, M.M.K.; supervision, M.M.K.; writing—original draft, H.M.A.-B.; writing—review and editing, M.M.K. All authors have read and agreed to the published version of the manuscript.

Funding: This research received no external funding.

Data Availability Statement: The data presented in this study are available on request from the corresponding author.

Conflicts of Interest: The authors declare no conflicts of interest.

References

1. Lamprecht, H.O. *Opus Caementitium: Bautechnik der Römer*; Beton-Verlag: Düsseldorf, Germany, 1996.
2. Ries, J.P.; Speck, J.; Harmon, K.S. *Lightweight Aggregate Optimizes the Sustainability of Concrete, Concrete Sustainability Conferences*; National Reading Mixed Concrete Association: Tucson, AZ, USA, 2010.
3. Topçu, I.B.; Uygunoğlu, T. Properties of autoclaved lightweight aggregate concrete. *Build. Environ.* **2006**, *42*, 4108–4116. [CrossRef]
4. Alarcon-Ruiz, L.; Platret, G.; Massieu, E.; Ehrlacher, A. The use of thermal analysis in assessing the effect of temperature on a cement paste. *Cem. Concr. Res.* **2004**, *35*, 609–613. [CrossRef]
5. Haddad, R.H.; Shannis, L.G. Post-fire behavior of bond between high strength pozzolanic concrete and reinforcing steel. *Constr. Build. Mater.* **2004**, *18*, 425–435. [CrossRef]
6. Zhu, Y.; Hussein, H.; Kumar, A.; Chen, G. A review: Material and structural properties of UHPC at elevated temperatures or fire conditions. *Cem. Concr. Compos.* **2021**, *123*, 104212. [CrossRef]
7. Kezmane, A.; Chiaia, B.; Kumpyak, O.; Maksimov, V.; Placidi, L. 3D modelling of reinforced concrete slab with yielding supports subject to impact load. *Eur. J. Environ. Civ. Eng.* **2017**, *21*, 988–1025. [CrossRef]
8. Scerrato, D.; Giorgio, I.; Della Corte, A.; Madeo, A.; Dowling, N.; Darve, F. Towards the design of an enriched concrete with enhanced dissipation performances. *Cem. Concr. Res.* **2016**, *84*, 48–61. [CrossRef]
9. *ISO 834–1*; Fire Resistance Tests-Elements of Building Construction. Part 1: General Requirements; ISO: Geneva, Switzerland, 1999.
10. Laurent, C. Investigating the fire resistance of ultra-lightweight foam concrete. *Rev. Técnica Fac. Ing. Univ. Zulia* **2014**, *37*, 11–18.
11. Kodur, V. Properties of Concrete at Elevated Temperatures. *ISRN Civ. Eng.* **2014**, *2014*, 1–15. [CrossRef]
12. Newman, J.; Owens, P. *Properties of Lightweight Concrete*; Materials Science, Engineering: Burlington, MA, USA, 2023.
13. Malhotra, H.L. The Effect of Temperature on the Compressive Strength of Concrete. *Mag. Concr. Res.* **1956**, *8*, 85–94. [CrossRef]
14. Shorter, G.W.; Harmathy, T.Z. Discussion on the article "NO beams" by Ashton and Bate. *Proc. Inst. Civ. Eng.* **1961**, *20*, 313.
15. Jansson, R. Fire spalling of concrete—A historical overview. *MATEC Web Conf.* **2013**, *6*, 01001. [CrossRef]
16. Domagała, L.; Hager, I. Influence of high temperature on compressive strength of structural lightweight concrete, Cement, Wapno, Beton. In Proceedings of the XVIII "Kontra" Conference, Kielce, Poland, 17–19 November 2023.
17. Křížová, K.; Bubeník, J.; Sedlmajer, M. Use of Lightweight Sintered Fly Ash Aggregates in Concrete at High Temperatures. *Buildings* **2022**, *12*, 2090. [CrossRef]
18. Adhikary, B.B.; Mutsuyoshi, H. Shear strengthening of RC beams with web-bonded continuous steel plates. *Constr. Build. Mater.* **2006**, *20*, 296–307. [CrossRef]
19. Zhou, J.; Wang, L. Repair of fire-damaged reinforced concrete members with axial load: A review. *Sustainability* **2019**, *11*, 963. [CrossRef]
20. Kog, Y.C. Practical Guide for the Assessment and Repair of Fire-Damaged Concrete Building Structures. *Pract. Period. Struct. Des. Constr.* **2021**, *26*, 04021010. [CrossRef]
21. Kumar, V.S.; Ariyannan, P. Retrofitting of RC beam using SIMCON laminate. *Int. J. Emerg. Technol. Comput. Sci. Electron.* **2016**, *20*, 219–225.
22. Sengul, O. Mechanical properties of slurry infiltrated fiber concrete produced with waste steel fibers. *Constr. Build. Mater.* **2018**, *186*, 1082–1091. [CrossRef]
23. Li, V.C. Engineered Cementitious Composites—Tailored Composites through Micromechanical Modeling. In *Fiber Reinforced Concrete: Present and the Future*; Banthia, N., Bentur, A., Mufti, A., Eds.; Canadian Society of Civil Engineers: Pointe Claire, QC, Canada, 1998.

24. Weimann, M.B.; Li, V.C. Hygral behavior of engineered cementitious composite (ECC). *Int. J. Restor. Build Monum.* **2003**, *9*, 513–534.
25. Li, V.C.; Leung, C.K.Y. Theory of steady-state and multiple cracking of random discontinuous fiber reinforced brittle matrix composites. *J. Eng. Mech.* **1992**, *118*, 2246–2264. [CrossRef]
26. Zhang, J.; Li, V.C. Monotonic and fatigue performance in bending of fiber-reinforced engineered cementitious composite in overlay system. *Cem. Concr. Res. Res* **2002**, *32*, 415–423. [CrossRef]
27. Ma, H.; Zhang, Z. Paving an engineered cementitious composite (ECC) overlay on concrete airfield pavement for reflective cracking resistance. *Constr. Build. Mater.* **2020**, *252*, 119048. [CrossRef]
28. Ahmadi, A.; Kianoush, M.R.; Moslemi, M.; Lachemi, M.; Siad, H.; Booya, E. Investigation on Repair of Tension Cracks in Reinforced Concrete Panels. *Eng. Struct.* **2021**, *245*, 112974. [CrossRef]
29. Kim, Y.Y.; Fischer, G.; Lim, Y.M.; Li, V.C. Mechanical Performance of Sprayed Engineered Cementitious Composite Using Wet-Mix Shotcreting Process for Repair Applications. *ACI Mater. J.* **2004**, *101*, 42–49.
30. *ASTM C330M-17a*; Standard Specification for Lightweight Aggregates for Structural Concrete. ASTM International: West Conshohocken, PA, USA, 2017.
31. *ACI 211.2-98*; Standard Practice for Selecting Proportions for Structural Lightweight Concrete. American Concrete Institute: Chicago, IL, USA, 1998.
32. *BS EN 197-1:201*; Cement: Composition, Specifications and Conformity Criteria for Common Cements. British Standards Institution: London, UK, 2019.
33. *BS EN 15167*; Ground Granulated Blast Furnace Slag for Use in Concrete, Mortar and Grout—Part 1: Definitions, Specifications and Conformity Criteria. British Standards Institution: London, UK, 2006.
34. *BS 3892-1:1997*; Pulverized-Fuel-Ash: Specification for Pulverized-Fuel-Ash for Use with Portland Cement. British Standards Institution: London, UK, 1997.
35. *BS EN 450-1:2012*; Fly Ash for Concrete—Definition, Specifications and Conformity Criteria. British Standards Institution: London, UK, 2012.
36. *ASTM, C494/C494M*; Standard Specification for Chemical Admixtures for Concrete. Annual Book of ASTM Standards: West Conshehoken, PA, USA, 2013.
37. Yuan, F.; Pan, J.L.; Wu, Y.F. Numerical study on 1exural behaviors of steel reinforced engineered cementitious composite (ECC) and ECC/concrete composite beams. *Sci. China Technol. Sci.* **2014**, *57*, 637–645. [CrossRef]
38. Deng, M.; Zhang, Y. Cyclic loading tests of RC columns strengthened with high ductile fiber reinforced concrete jacket. *Constr. Build. Mater.* **2017**, *153*, 986–995. [CrossRef]
39. Lee, J.-H.; Cho, B.; Choi, E. Flexural Capacity of Fiber Reinforced Concrete with a Consideration of Concrete Strength and Fiber Content. *Constr. Build. Mater.* **2017**, *138*, 222–231. [CrossRef]
40. Li, V.C. Engineered Cementitious Composites (ECC)—Material, Structural, and Durability Performance. In *Concrete Construction Engineering Handbook*; Nawy, E., Ed.; CRC Press: Boca Raton, FL, USA, 2008; Chapter 24.
41. Azizinamini, A.; Pavel, R.; Hatfield, E.; Gosh, S.K. The behavior of lap-spliced reinforcing bars embedded in high-strength concrete. *ACI Struct. J.* **1999**, *96*, 826–836. [CrossRef]
42. Şahmaran, M.; Li, V.C. Durability properties of microcracked ECC containing high volumes fly ash. *Cem. Concr. Res.* **2009**, *39*, 1033–1043. [CrossRef]
43. Wang, S.; Li, V.C. Engineered cementitious composites with high-volume fly ash. *ACI Mater. J.* **2007**, *104*, 233–241.

Disclaimer/Publisher's Note: The statements, opinions and data contained in all publications are solely those of the individual author(s) and contributor(s) and not of MDPI and/or the editor(s). MDPI and/or the editor(s) disclaim responsibility for any injury to people or property resulting from any ideas, methods, instructions or products referred to in the content.